

Nonlinear Double Compton Scattering in the Ultrarelativistic Quantum Regime

F. Mackenroth and A. Di Piazza*

Max-Planck-Institut für Kernphysik, Saupfercheckweg 1, 69117 Heidelberg, Germany

(Received 16 August 2012; published 11 February 2013)

A detailed analysis of the process of two-photon emission by an electron scattered from a high-intensity laser pulse is presented. The calculations are performed in the framework of strong-field QED and include exactly the presence of the laser field described as a plane wave. We investigate the full nonlinear quantum regime of interaction with a few-cycle pulse, where nonlinear effects in the laser field amplitude, photon recoil, and the short pulse duration substantially alter the emitted photon spectra as compared to those in previously studied regimes. We provide a semiclassical explanation for such differences, based on the possibility of assigning a trajectory to the electron in the laser field before and after each quantum photon emission. Our numerical results indicate the feasibility of investigating experimentally the full ultrarelativistic quantum regime of nonlinear double Compton scattering with available electron accelerator and laser technology.

DOI: [10.1103/PhysRevLett.110.070402](https://doi.org/10.1103/PhysRevLett.110.070402)

PACS numbers: 12.20.Ds, 41.60.-m

Electromagnetic radiation by accelerated charged particles is one of the most fundamental processes in physics, and it is exploited experimentally for different purposes ranging from the generation of coherent x rays [1] to the production of multi-GeV photon beams [2] and medical applications. It is also a useful tool for investigating fundamental physics and, for example, it has played a crucial role for testing the validity of the high-energy sector of QED [3]. In classical electrodynamics, a charge, an electron for definiteness (mass m and charge $e < 0$, respectively), radiates only if it is accelerated. Analogously, quantum mechanically photon emission can occur only if the electron absorbs at least one photon. When an electron is driven by an intense electromagnetic field, the emission of photons may occur with the absorption of many photons from the field.

High-power lasers are irreplaceable tools to test the high-intensity sector of QED, as complementary to the high-energy one [4]. The effects of a laser field approximated as a plane wave have to be taken into account exactly if $\xi = |e|\mathcal{E}_0/mc\omega_0 \gtrsim 1$, where \mathcal{E}_0 is the electric field amplitude of the field and ω_0 its central angular frequency. The threshold $\xi \approx 1$ corresponds to an optical ($\hbar\omega_0 \approx 1$ eV) laser intensity of about 10^{18} W/cm² whereas available ones exceed already 10^{22} W/cm² [5]. The emission of a single photon by an electron in a plane wave [nonlinear single Compton scattering (NSCS)] has been thoroughly investigated theoretically (see the recent review [4]) and the QED predictions at $\xi \lesssim 1$ have been confirmed experimentally [6]. Recent studies on NSCS have been focused on finite-pulse effects and especially on the high-intensity regime $\xi \gg 1$, where a large number ($\sim \xi^3$) of laser photons is absorbed by the electron during the emission process [7–11]. In addition to ξ , NSCS is characterized by the parameter $\chi = ((k_0 p_i)/m\omega_0) \times (\mathcal{E}_0/\mathcal{E}_{\text{cr}})$, where $k_0^\mu = (\omega_0/c, \mathbf{k}_0)$ is the four-wave-vector

of the laser photons ($|\mathbf{k}_0| = \omega_0/c$), $p_i^\mu = (\varepsilon_i/c, \mathbf{p}_i)$ is the initial electron four-momentum, and $\mathcal{E}_{\text{cr}} = m^2 c^3 / \hbar |e| = 1.3 \times 10^{16}$ V/cm [4]. The parameter χ controls quantum effects like the photon recoil, and at $\chi \ll 1$ the NSCS spectra coincide with the classical ones [12]. The emission of two photons by an electron in a plane wave [nonlinear double Compton scattering (NDCS)] allows for studying correlation effects in the emitted radiation, and it has also been investigated with an emphasis on the entanglement of the two emitted photons [13] and on the relative yield between NSCS and NDCS [14]. Both these studies have been focused on the radiation regime where $\xi \sim 1$, such that the electron absorbs only a few photons from the laser field (“quasilinear” regime) [4], and where $\chi \ll 1$, such that quantum photon recoil was negligible. At $\xi \sim 1$ the condition for the importance of recoil is essentially $\hbar(k_0 p_i)/m^2 c^2 \sim 1$ (see Ref. [15]), as in the linear regime, i.e., in double Compton scattering by a gamma photon, which was already measured [16].

In the present Letter we investigate NDCS in a few-cycle laser pulse in the full ultrarelativistic quantum regime $\xi \gg 1$, $\chi \gtrsim 1$ including exactly the effects of the plane wave. As a result of the localized nature of photon emission, of highly nonlinear effects in the laser amplitude, of photon recoil, and of the short pulse duration, the physics of NDCS and the emission spectra here substantially differ from those in the quasilinear regime ($\xi \sim 1$) at $\chi \ll 1$ studied in Refs. [13,14] for a monochromatic and in detail for a many-cycle plane wave, respectively [17]. We explain the new features of the emission spectra by developing a quasiclassical approach, where a trajectory is assigned to the electron in the laser field, with discontinuities in the electron energy due to the quantum emission of photons. Finally, we show numerically that the studied regime can be entered already with experimentally demonstrated laser intensities of the order of 10^{21} W/cm² [5], together with

high-energy electron beams generated by either available conventional accelerators [18] or present-generation laser-based accelerators [19].

We consider a linearly polarized plane-wave field described by the four-potential $A_0^\mu(\eta) = (\mathcal{E}_0/\omega_0)\epsilon_0^\mu\psi(\eta)$, where ϵ_0^μ is the wave's polarization four-vector and the shape function $\psi(\eta)$ depends on the space-time coordinates x^μ only via the invariant phase $\eta = (k_0x)$ (units with $\hbar = c = 1$ are used throughout). For a generic four-vector $a^\mu = (a^0, \mathbf{a})$ we introduce the light-cone representation $a^\mu = (a^+, a^-, \mathbf{a}^\perp)$, where $a^\pm = (a^0 \pm a^\parallel)/\sqrt{2}$, with $a^\parallel = \mathbf{k}_0 \cdot \mathbf{a}/\omega_0$, and where $\mathbf{a}^\perp = \mathbf{a} - a^\parallel \mathbf{k}_0/\omega_0$. In the Furry picture of QED, the electron wave functions in the presence of a plane-wave field are the so-called Volkov wave functions [20]. The Volkov wave function for an electron with four-momentum p^μ and spin quantum number σ outside the plane wave has the form $\Psi_{p,\sigma}(x) = E_p(x)u_{p,\sigma}/\sqrt{2\varepsilon}$, where $u_{p,\sigma}$ is a free bispinor, a unity quantization volume is assumed, and the Ritus matrices

$$E_p(x) = \left[1 + \frac{e\mathbf{k}_0 A_0(\eta)}{2(k_0 p)} \right] \times e^{-i\{(px) + \int_0^\eta d\phi \{e[pA_0(\phi)]/(k_0 p)\} - [e^2 A_0^2(\phi)/2(k_0 p)]\}} \quad (1)$$

have been introduced, with $\hat{a} = \gamma^\mu a_\mu$ for the Dirac matrices γ^μ . We consider an electron with initial (final) four-momentum $p_i^\mu = (\varepsilon_i, \mathbf{p}_i)$ ($p_f^\mu = (\varepsilon_f, \mathbf{p}_f)$) and spin quantum number σ_i (σ_f), which emits two photons with four-momenta k_1^μ and k_2^μ and with polarization four-vectors $\epsilon_{k_1, \lambda_1}^\mu$ and $\epsilon_{k_2, \lambda_2}^\mu$, respectively. The scattering matrix element S_{fi} of this process can be written as $S_{fi}^{(1)} + S_{fi}^{(2)}$, where (see Fig. 1)

$$S_{fi}^{(1)} = -e^2 \int d^4x d^4y \bar{\Psi}_{p_f, \sigma_f}(y) \epsilon_{k_2, \lambda_2}^* e^{i(k_2 y)} \times G(y, x) \epsilon_{k_1, \lambda_1}^* e^{i(k_1 x)} \Psi_{p_i, \sigma_i}(x) \quad (2)$$

and $S_{fi}^{(2)} = S_{fi}^{(1)}(1 \leftrightarrow 2)$. In Eq. (2) $\bar{\Psi}_{p,\sigma}(x) = \Psi_{p,\sigma}^\dagger(x)\gamma^0$, and

$$G(y, x) = \lim_{\epsilon \rightarrow 0} \int \frac{d^4p}{(2\pi)^4} E_p(y) \frac{\not{p} + m}{p^2 - m^2 + i\epsilon} \bar{E}_p(x) \quad (3)$$

with $\bar{E}_p(x) = \gamma^0 E_p^\dagger(x)\gamma^0$ is the Volkov propagator [15]. We analyze here only the quantity $S_{fi}^{(1)}$. The structure of the Ritus matrices allows us to perform the integrations in x^\pm

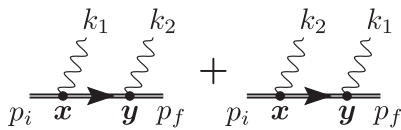


FIG. 1. Tree-level Feynman diagrams of NDCS in the Furry picture. The double solid lines represent Volkov states and propagators.

and x^\perp (y^+ and y^\perp), which provide the energy-momentum conservation laws $p_i^\perp = k_1^\perp + p_f^\perp$ and $p_i^- = k_1^- + p_f^-$ ($p_i^\perp = k_2^\perp + p_f^\perp$ and $p_i^- = k_2^- + p_f^-$). One of these sets of conservation laws can be employed to perform three integrations in $G(y, x)$. The only remaining integral in Eq. (3) is

$$I(y^-, x^-) = \lim_{\epsilon \rightarrow 0} \int \frac{d^4p}{2\pi} \frac{\not{p} + m}{p^+ - p_i^+ + i\epsilon} e^{ip^+(x^- - y^-)} = \not{p}_0 \delta(x^- - y^-) - i(\not{p}_i + m)\Theta(y^- - x^-), \quad (4)$$

where $n_0^\mu = k_0^\mu/\omega_0$, $\Theta(\cdot)$ is the step function and where the four-momentum p_i^μ has light-cone coordinates $p_i^- = p_i^- - k_1^- = k_2^- + p_f^-$, $\mathbf{p}_i^\perp = \mathbf{p}_i^\perp - \mathbf{k}_1^\perp = \mathbf{k}_2^\perp + \mathbf{p}_f^\perp$, and $p_i^+ = (\mathbf{p}_i^\perp{}^2 + m^2)/2p_i^-$ (note that $p_i^2 = m^2$). The above decomposition allows us to write the quantity $S_{fi}^{(1)}$ as $S_{fi}^{(1)} = (2\pi)^3 \delta(p_i^- - k_1^- - k_2^- - p_f^-) \delta^2(\mathbf{p}_i^\perp - \mathbf{k}_1^\perp - \mathbf{k}_2^\perp - \mathbf{p}_f^\perp) \times \sum_{r,s=0}^2 (a_r f_r \delta_{r,s} + b_{r,s} f_{r,s})$, where the coefficients a_r and $b_{r,s}$ are matrix factors whose exact form is not needed here. In fact, all the dynamical information on the process is contained in the functions

$$f_r = \int d\eta \psi^r(\eta) \exp\{-i[S_x(\eta) + S_y(\eta)]\}, \quad (5a)$$

$$f_{r,s} = \int d\eta_x d\eta_y \Theta(\eta_y - \eta_x) \psi^s(\eta_x) \psi^r(\eta_y) \times \exp\{-i[S_x(\eta_x) + S_y(\eta_y)]\}, \quad (5b)$$

where $S_{x/y}(\eta) = \int_0^\eta d\eta' [\alpha_{x/y} \psi(\eta') + \beta_{x/y} \psi^2(\eta') + \gamma_{x/y}]$, with $\alpha_x = -m\xi[(p_i \epsilon_0)/(k_0 p_i) - (p_f \epsilon_0)/(k_0 p_f)]$, $\beta_x = -m^2 \xi^2 (k_0 k_1)/2(k_0 p_i)(k_0 p_f)$, $\gamma_x = -(k_1 p_i)/(k_0 p_i)$, and with α_y , β_y , and γ_y obtained from α_x , β_x , and γ_x , respectively, with the substitutions $p_i^\mu \rightarrow p_f^\mu$, $p_i^\mu \rightarrow p_i^\mu$, and $k_1^\mu \rightarrow k_2^\mu$. We call ‘‘coherent’’ (‘‘incoherent’’) the contributions to the amplitude $S_{fi}^{(1)}$ containing the functions f_r ($f_{r,s}$). The divergences in the integrals, which do not contain the shape function $\psi(\eta)$ in the prefactor, can be avoided by employing the identities [8,14,21] $\gamma_y f_{0,s} = -if_s - (\alpha_y f_{1,s} + \beta_y f_{2,s})$, $\gamma_x f_{r,0} = if_r - (\alpha_x f_{r,1} + \beta_x f_{r,2})$, and $(\gamma_x + \gamma_y) f_0 = -(\alpha_x + \alpha_y) f_1 - (\beta_x + \beta_y) f_2$. The differential average energy emitted dE , summed (averaged) over all outgoing (incoming) discrete quantum numbers is given by

$$dE = \frac{\omega_1 + \omega_2}{2} \frac{d^3 p_f}{(2\pi)^3} \prod_{i=1}^2 \frac{d^3 k_i}{(2\pi)^3} \sum_{\{\sigma, \lambda\}} |S_{fi}^{(1)} + S_{fi}^{(2)}|^2, \quad (6)$$

where $\{\sigma, \lambda\} \equiv \sigma_i, \sigma_f, \lambda_1, \lambda_2$. Note that the three δ functions contained in $S_{fi}^{(1)}$ [and in $S_{fi}^{(2)}$] can be exploited to perform the integrations in \mathbf{p}_f .

We consider a few-cycle laser pulse propagating along the positive z axis polarized along the x direction, and an electron initially counterpropagating with respect to the laser beam, i.e., $\mathbf{p}_i = (0, 0, -\beta_i \varepsilon_i)$ with $\beta_i > 0$. The shape

function is $\psi(\eta) = \sin^4(\eta/4)\sin(\eta)$ for $\eta \in [0, 4\pi]$ and zero elsewhere, corresponding to a two-cycle pulse of approximately 5-fs duration at $\omega_0 = 1.55$ eV. We first consider a laser system with peak intensity $I_0 = 5 \times 10^{20}$ W/cm² ($\xi \approx 15$). In this regime the electron absorbs about $\xi^3 \sim 3000$ laser photons during each emission process [8,15], indicating a highly nonlinear dependence of the process itself on the laser amplitude.

In order to highlight qualitative differences between the full quantum regime $\chi \sim 1$ considered here and the already-studied regime at $\chi \ll 1$, we first report on a numerical example within the latter. Thus, we set $\varepsilon_i = 40$ MeV, which corresponds to $\chi = 5 \times 10^{-3}$. We choose to observe one photon at $\theta_1 = \pi - \theta_0/2$ with $\theta_0 = m\xi/\varepsilon_i$, and the other one at the two different polar angles $\theta_2 = \theta_1$ [see Fig. 2(a)] and $\theta_2 = \pi - 1.1\theta_0$ [see Fig. 2(b)]. Also, we choose $\phi_1 = \pi$, $\phi_2 = 0$ in both cases as azimuthal observation angles. For our pulse shape $\psi(\eta)$, (1) the emission cone of NSCS is determined by the condition $\pi - \theta \leq \psi_0\theta_0$ on the polar angle θ with $\psi_0 = |\max(\psi(\eta))| = 0.8$ [22], and (2) the NSCS emission spectra at $(\theta, \phi = 0)$ and at $(\theta, \phi = \pi)$ coincide. Therefore, if $\theta_2 = \theta_1$ both photons are observed within

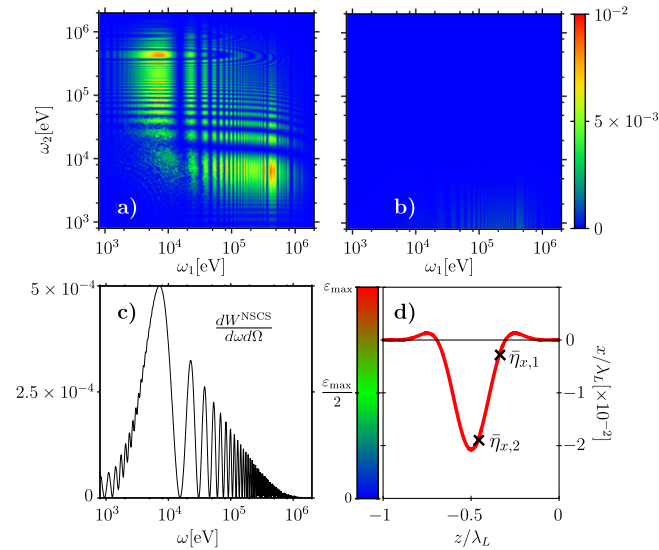


FIG. 2 (color online). Two-photon energy emission spectra $dE/\Pi_{i=1}^2 d\omega_i d\Omega_i$ [eV⁻¹ sr⁻²] at $\chi = 5 \times 10^{-3}$ observed at $\theta_1 = \pi - \theta_0/2$, and at $\theta_2 = \theta_1$ (a) and at $\theta_2 = \pi - 1.1\theta_0$ (b), with $\theta_0 = 0.19$ rad. The other numerical parameters are given in the text. (c): NSCS emission probability $dW^{\text{NSCS}}/d\omega d\Omega$ [eV⁻¹ sr⁻¹] at (θ_1, ϕ_1) . (d): Classical electron trajectories (the instantaneous electron energy is color encoded) with initial four-momenta p_i^μ and p_f^μ joined at $\bar{\eta}_{x,1}$. Since as a typical photon emission energy, the value 10^5 eV has been chosen [see (a) and (c)], then $p_i^\mu \approx p_f^\mu$ and the two trajectories are indistinguishable. ε_{max} is the maximum electron energy in the laser field. The crosses mark the points of the trajectory where the classical electron's velocity is along (θ_1, ϕ_1) .

the emission cone of NSCS, whereas if $\theta_2 = \pi - 1.1\theta_0$ one of the photons is observed outside this cone.

A comparison of Figs. 2(a) and 2(b) shows that the radiation outside the NSCS emission cone is negligibly small relative to that within this cone. This feature can be quantitatively understood by virtue of a stationary-phase analysis [8,15]. In fact, at $m\xi$, $\varepsilon_i \gg m$ the phases in the integrands in Eq. (5a) and (5b) are of the order of $\xi^3 \gg 1$ [8,15], and the saddle-point method can be applied. In the NSCS analysis of an electron with initial momentum p_i emitting a photon with wave vector k , for $\xi \gg 1$ the saddle points $\bar{\eta}_l$ are almost real ($|\text{Im}(\bar{\eta}_l)/\text{Re}(\bar{\eta}_l)| \sim 1/\xi$) and $\text{Re}(\bar{\eta}_l)$ corresponds to those phase instants where the classical electron momentum points along k [8]. Accordingly, the overall emission cone corresponds to the angular region covered by the electron's classical velocity vector along its complete classical trajectory in the laser pulse. Thus, the electron propagation in the laser field is quasiclassical and the photon recoil is the main quantum effect to be accounted for Ref. [23]. Now, we have checked numerically that the NDCS spectrum is dominated by the contribution proportional to the functions $f_{r,s}$. These integrals, according to the saddle-point method, can be approximated as $f_{r,s} \approx \sum_{l,n} \Theta(\bar{\eta}_{y,n} - \bar{\eta}_{x,l}) f_r^y(\bar{\eta}_{y,n}) f_s^x(\bar{\eta}_{x,l})$. Here, the indices l and n run over all stationary points, which are found as solutions of the equations $dS_{x/y}(\eta)/d\eta|_{\eta=\bar{\eta}_{x,l/y,n}} = 0$ and $f_r^{x/y} = \int d\eta \psi^r(\eta) \exp[-iS_{x/y}(\eta)]$ [see Eq. (5b)]. The above-approximated expression of $f_{r,s}$ can be interpreted as a two-step emission process in which the electron first emits a photon with four-momentum k_1^μ changing its own four-momentum from p_i^μ to p_f^μ , and then it emits a photon with four-momentum k_2^μ changing its own four-momentum from p_f^μ to p_f^μ (recall that the total amplitude also contains a term with the photon indices 1 and 2 exchanged). One can picture this dynamics by considering a succession of two classical trajectories with initial four-momenta p_i^μ and p_f^μ , respectively, continuously joined at a point corresponding to the phase $\bar{\eta}_{x,l}$, where the photon with four-momentum k_1^μ is emitted. In Fig. 2(d) we show in principle a pair of such classical electron trajectories joined at the point marked with a cross and labeled as $\bar{\eta}_{x,1}$, where the electron propagates along the observation direction (θ_1, ϕ_1) . However, since in the regime $\chi \ll 1$ the recoil is negligible [see Figs. 2(a) and 2(c) and recall that $\varepsilon_i = 40$ MeV], the two four-momenta p_i^μ and p_f^μ are practically identical and the two trajectories are indistinguishable [in Fig. 2(d) we subtracted the momentum of a typical photon of energy $\omega_1 = 10^5$ eV emitted towards (θ_1, ϕ_1) from the initial electron momentum, see Figs. 2(a) and 2(c)]. The same occurs if the two trajectories are joined at the other saddle point $\bar{\eta}_{x,2}$ [see Fig. 2(d)], where the electron's velocity is again along the observation direction (θ_1, ϕ_1) . Analytically, by inserting the parameters α_x and β_x (α_y and β_y), the stationary-point equation at the vertex x (y) provides

$\psi(\bar{\eta}_x) = -1/2$ ($\psi(\bar{\eta}_y) = \Delta\vartheta_2 - (\omega_1/\varepsilon_i)(1/2 + \Delta\vartheta_2)$), with $\Delta\vartheta_2 = (\pi - \theta_2)/\theta_0$. If photon recoil is negligible ($\omega_1 \ll \varepsilon_i$), the condition for $\bar{\eta}_y$ has a real solution only if $\Delta\vartheta_2 < \psi_0$, i.e., only if θ_2 lies within the NSCS emission cone. This explains the negligible emission outside this cone in Fig. 2(b).

Also, by comparing the frequency distribution of the NDCS emission spectrum in Fig. 2(a) with the NSCS emission probability $dW^{\text{NSCS}}/d\omega d\Omega$ [7–9] in Fig. 2(c), it is apparent that the NDCS spectrum for $\chi \ll 1$ (and $\xi \gg 1$) corresponds to an emission probability given by the “product” of two independent NSCS probability distributions for each photon [the maximum in the probability in Fig. 2(c) is at lower energies than in the NDCS emission spectrum in Fig. 2(a), as the latter contains an additional factor $\omega_1 + \omega_2$]. While the formation length ℓ of NSCS in a few-cycle pulse at $\xi \sim 1$ [13,14] is of the order of the laser’s pulse length, at $\xi \gg 1$ it is even much smaller than the laser’s central wavelength $\lambda_0 = 2\pi/\omega_0$, as it holds $\ell \sim \lambda_0/\xi$ [4]. Thus, for $\xi \gg 1$ each photon emission is well localized and, if recoil effects can be neglected, the two-photon emission process can essentially be described by two independent NSCS events [24]. Accordingly, we checked that if W^{NDCS} (W^{NSCS}) is the total NDCS (NSCS) emission probability, then $W^{\text{NDCS}} \approx (W^{\text{NSCS}})^2/2$ [24].

Finally, the positions of the spectral peaks in Fig. 2(a) significantly differ from those in a many-cycle pulse [14], which essentially correspond to the so-called Oleinik resonances rigorously occurring only in a monochromatic wave [13]. For example, the first emission peak here is at about 10 keV [see Fig. 2(c)], whereas the first Oleinik resonance would be at about 215 eV.

The physical situation, however, changes substantially if we enter the full quantum regime at $\chi \sim 1$. In order to investigate this regime, we set $\varepsilon_i = 2.5$ GeV [25], and $I_0 = 3 \times 10^{21}$ W/cm², resulting in $\chi = 1.1$, and keep all other parameters unchanged with respect to the above example. Here, $\xi \approx 37$ and the electron absorbs about $\xi^3 \sim 5 \times 10^4$ laser photons during each emission process. By observing the two emitted photons at the same emission angles as before [see Figs. 3(a) and 3(b)], we note that (1) the quantum mechanical cutoff energy for the sum of the emitted photons’ energies, approximately given by the equation $\omega_1 + \omega_2 = \varepsilon_i$, is well approached, (2) since in the quantum regime the electron loses a substantial part of its energy after the emission of the first photon, the asymmetry in the energies of the two emitted photons [see Fig. 3(a)] is much more pronounced than at $\chi \ll 1$ [see Fig. 2(a)], and (3) the electron also emits outside of the NSCS emission cone [see Fig. 3(b) and note that $\theta_0 = 7.6 \times 10^{-3}$ rad for the present numerical parameters].

The third feature is particularly important as it allows us to measure NDCS in the full ultrarelativistic quantum regime. To explain it qualitatively, we show in Fig. 3(c) the classical trajectories for initial momenta \mathbf{p}_i (solid line)

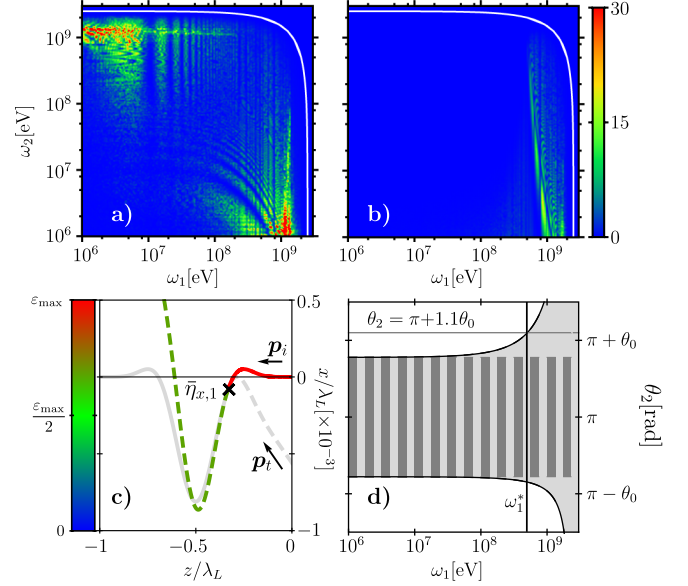


FIG. 3 (color online). Two-photon energy emission spectra $dE/\Pi_{i=1}^2 d\omega_i d\Omega_i$ [eV⁻¹sr⁻²] at $\chi \approx 1.1$ observed at $\theta_1 = \pi - \theta_0/2$, and at $\theta_2 = \theta_1$ (a) and at $\theta_2 = \pi - 1.1\theta_0$ (b), with $\theta_0 = 7.6 \times 10^{-3}$ rad. The other numerical parameters are given in the text. The solid white lines correspond to the cutoff-energy equation $\omega_1 + \omega_2 = \varepsilon_i$. (c): The two classical electron trajectories with initial electron momentum \mathbf{p}_i (solid line) and \mathbf{p}_t (dashed line). The color-encoded line shows the actual electron trajectory for a photon with energy $\omega_1 = 0.8$ GeV and momentum along (θ_1, ϕ_1) emitted at $\bar{\eta}_{x,1}$. (d): Emission opening angle for the second emitted photon as a function of ω_1 (light shaded area) compared with the emission cone for NSCS with initial electron momentum \mathbf{p}_i (dark stripes). The vertical line indicates the value $\omega_1 = \omega_1^*$ described in the text.

and \mathbf{p}_t (dashed line) obtained for the emission of a photon of energy $\omega_1 = 0.8$ GeV and momentum along (θ_1, ϕ_1) at $\bar{\eta}_{x,1}$ (the analysis in the case in which the electron emits at $\bar{\eta}_{x,2}$ is analogous). At this value of ω_1 the emission probability is maximal. The derivatives of the two trajectories coincide at $\bar{\eta}_{x,1}$ [see Fig. 3(c)], as the photon is assumed to be emitted with momentum parallel to the instantaneous electron’s velocity. However, the color coding shows that the electron energy discontinuously decreases at $\bar{\eta}_{x,1}$ due to photon recoil. The abrupt energy decrease induces a stronger deflection of the electron trajectory in the laser field after the photon emission. Thus, the resulting emission cone’s opening angle increases, and the emission outside of the NSCS emission cone becomes possible. The same conclusion can be drawn analytically, evaluating the saddle-point equation $\psi(\bar{\eta}_y) = \Delta\vartheta_2 - (\omega_1/\varepsilon_i)(1/2 + \Delta\vartheta_2) \leq \psi_0$, with $\Delta\vartheta_2 = (\pi - \theta_2)/\theta_0$. Solving the latter inequality for θ_2 , we obtain an expression for the cutoff angles of the second photon emission as a function of ω_1 [see Fig. 3(d) with $\phi_2 = 0$ mapped to $\theta_2 > \pi$ and $\phi_2 = \pi$ mapped to $\theta_2 < \pi$]. The photon-energy threshold ω_1^* , beyond which emission along $\theta_2 = \pi + 1.1\theta_0$ becomes

possible [see Fig. 3(b)], is well reproduced by this analytical prediction [see Fig. 3(d)]. Thus, measuring MeV photons outside of the NSCS emission cone would reveal a NDCS signal, where NSCS is exponentially suppressed and negligible. The emission probability outside of the NSCS emission cone results to be of the order of 0.1, indicating the observability in principle of the process employing laser-generated electron beams, which typically contain $\sim 10^8$ electrons [19]. In order to resolve detailed spectral signatures of the photon spectra, however, electron beams with much smaller normalized emittance and relative energy spread, such as available at conventional accelerators [18], are required [26]. In general, it is not possible experimentally to separate the coherent contribution to the amplitude from the incoherent one. However, we have checked numerically that in the above example the coherent contribution is negligibly small. Finally, NSCS and NDCS photons may create electron-positron pairs, which in turn would generate a radiation background for NDCS itself. However, Figs. 3(a) and 3(b) and analogous results for NSCS spectra indicate that photons are produced here with energy $\omega \approx 1.5$ GeV, and this background radiation is suppressed by a factor $\exp(-8\varepsilon_i/3\omega\chi) \approx 10^{-2}$ [4].

The authors acknowledge useful discussions with A. Ilderton, D. Seipt, and B. Kämpfer.

*dipiazza@mpi-hd.mpg.de

- [1] R. Moshhammer and J. Ullrich, *J. Phys. B* **42**, 130201 (2009).
- [2] A. Apyan *et al.*, *Nucl. Instrum. Methods Phys. Res., Sect. B* **234**, 128 (2005).
- [3] P. Achard *et al.*, *Phys. Lett. B* **616**, 145 (2005).
- [4] A. Di Piazza, C. Müller, K. Z. Hatsagortsyan, and C. H. Keitel, *Rev. Mod. Phys.* **84**, 1177 (2012).
- [5] V. Yanovsky *et al.*, *Opt. Express* **16**, 2109 (2008).
- [6] C. Bula *et al.*, *Phys. Rev. Lett.* **76**, 3116 (1996); C. Bamber *et al.*, *Phys. Rev. D* **60**, 092004 (1999).
- [7] M. Boca and V. Florescu, *Phys. Rev. A* **80**, 053403 (2009).
- [8] F. Mackenroth and A. Di Piazza, *Phys. Rev. A* **83**, 032106 (2011).
- [9] D. Seipt and B. Kämpfer, *Phys. Rev. A* **83**, 022101 (2011).
- [10] K. Krajewska and J. Z. Kamiński, *Phys. Rev. A* **85**, 062102 (2012).
- [11] C. Harvey, T. Heinzl, A. Ilderton, and M. Marklund, *Phys. Rev. Lett.* **109**, 100402 (2012).
- [12] J. D. Jackson, *Classical Electrodynamics* (John Wiley & Sons, New York, 1962).
- [13] E. Lötstedt and U. D. Jentschura, *Phys. Rev. A* **80**, 053419 (2009); *Phys. Rev. Lett.* **103**, 110404 (2009).
- [14] D. Seipt and B. Kämpfer, *Phys. Rev. D* **85**, 101701 (2012).
- [15] V. I. Ritus, *J. Sov. Laser Res.* **6**, 497 (1985).
- [16] P. E. Cavanagh, *Phys. Rev.* **87**, 1131 (1952); M. B. Saddi, B. S. Sandhu, and B. Singh, *Ann. Nucl. Energy* **33**, 271 (2006).
- [17] Note that the general theory presented in Ref. [14], as the one formulated here, applies to an arbitrary linearly polarized plane-wave field.
- [18] I. V. Bazarov *et al.*, in *Proceedings of the Particle Accelerator Conference* (IEEE, Chicago, Illinois, 2001), p. 230.
- [19] W. P. Leemans, B. Nagler, A. J. Gonsalves, Cs. Tóth, K. Nakamura, C. G. R. Geddes, E. Esarey, C. B. Schroeder, and S. M. Hooker, *Nat. Phys.* **2**, 696 (2006); C. E. Clayton *et al.*, *Phys. Rev. Lett.* **105**, 105003 (2010).
- [20] V. B. Berstetskii, E. M. Lifshitz, and L. P. Pitaevskii, *Quantum Electrodynamics* (Elsevier, Oxford, 1982).
- [21] A. Ilderton, *Phys. Rev. Lett.* **106**, 020404 (2011).
- [22] F. Mackenroth, A. Di Piazza, and C. H. Keitel, *Phys. Rev. Lett.* **105**, 063903 (2010).
- [23] V. N. Baier, V. M. Katkov, and V. M. Strakhovenko, *Electromagnetic Processes at High Energies in Oriented Single Crystals* (World Scientific, Singapore, 1998).
- [24] R. J. Glauber, *Phys. Rev.* **84**, 395 (1951).
- [25] S. Y. Kalmykov *et al.*, *High Energy Density Phys.* **6**, 200 (2010).
- [26] F. V. Hartemann, D. J. Gibson, W. J. Brown, A. Rousse, K. Ta Phuoc, V. Mallka, J. Faure, and A. Pukhov, *Phys. Rev. ST Accel. Beams* **10**, 011301 (2007).